Appl Nanosci (2016) 6:121–129
DOI 10.1007/s13204-015-0422-x

ORIGINAL ARTICLE

Characterization and in vitro studies on anticancer, antioxidant activity against colon cancer cell line of gold nanoparticles capped with *Cassia tora* SM leaf extract

Ezra Elumalai Abel · Preetam Raj John Poonga · Shirly George Panicker

Received: 27 January 2015 / Accepted: 11 February 2015 / Published online: 22 February 2015

Abstract This study was aimed to determine the effectiveness of synthesized gold nanoparticles of an ethnobotanically and medicinally important plant species *Cassia tora* against colon cancer cells and to find its antibacterial and antioxidant activities. In order to improve the bioavailability of *C. tora*, we synthesized gold nanoparticles through green synthesis, by simple mixing and stirring of *C. tora* leaf powder and tetrachloroauric acid ($HAuCl_4$) solution which gave a dispersion of gold nanoparticles conjugate with *C. tora* secondary metabolites (SMs) with characteristic surface plasmon resonance. It was characterized by Fourier transform infrared spectroscopy, zeta sizer, zeta potential and transmission electron microscopy. Antibacterial activity was carried out for gold nanoparticles conjugated with *C. tora* SMs, using well-diffusion method. The MTT assay for cell viability and markers such as catalase, nitric oxide and lipid peroxidation was predictable to confirm the cytotoxicity and antioxidant properties. The treatment of gold nanoparticles conjugated with *C. tora* SMs on Col320 cells showed reduction in the cell viability through MTT assay, and it also significantly suppressed the release of H_2O_2, LPO and NO production in a dose-dependent manner. *C. tora* SMs conjugate gold nanoparticles showed enhanced bioavailability, antioxidant and anticancer effect against colon cancer cell line (Col320).

Keywords Antibacterial · Anticancer · Antioxidants · FT-IR · AuNps · *C. tora* SMs

E. E. Abel (✉) · P. R. John Poonga (✉) · S. G. Panicker
Department of Plant Biology and Biotechnology, PG Biotechnology, Loyola College, Chennai 600 034, Tamil Nadu, India
e-mail: loyolaezra@gmail.com

P. R. John Poonga
e-mail: preetamraj.jp@gmail.com

S. G. Panicker
Helen Keller Research Center, Loyola College, Chennai, Tamil Nadu, India

Introduction

The nature has provided the storehouse of remedies to cure many ailments of mankind. The traditional herbal medicines are still practiced in large part of our country mostly in tribal and rural areas. In many developing countries, large section of population relies on traditional medicinal plants since they contain active constituents that are used in the treatment of many human diseases (Stary and Hans 1998). *Cassia tora* Linn. Family: Caesalpiniaceae is an annual herb, 30–39 cm high, growing in India as wasteland rainy season weed. These herbs have been reported for their usefulness in the form of decoctions, infusions and tinctures in traditional system of medicines for treating skin diseases like psoriasis, leprosy and many more (Horvath 1992; Zahra et al. 2000; Cordova et al. 2002; Harrison 2003). *C. tora* was also reported for the presence of phytochemical such as anthraquinones, carbohydrates, glycosides, cardiac glycosides, amino acid, phytosterols, fixed oils and fats, phenolic compounds, tannins, flavonoids, steroids and saponins (Sathya and Ambikapathy 2012). And with high anthraquinone content, including chrysophanol, physcion and obtusin may aid in cancer prevention (Qi 2011). At present scenario, the pharmaceutical research has focused on the potent activities of *C. tora*, including its anti-aging, anticancer and antioxidant effects (Chen et al. 2014). Hence, the current study was intended to use *C. tora* as a bioreductant and capping agent for the synthesis of

gold nanoparticles as a promising carrier and therapeutic drug for cancer.

The biologically inspired experimental processes for the synthesis of nanoparticles are evolving into an important branch of nanotechnology. Gold nanoparticles have advantages over other metal nanoparticles due to their biocompatibility and non-cytotoxicity. Nanoparticles are nanometers in size. Gold is used internally in human for the last five decades due to their chemical inertness. These are also used in chemotherapy and diagnosis of cancer cell (Cai and Chen 2007). Biological synthesis of nanoparticles appears to be simple, cost-effective, non-toxic and easy to use for controlling size, shape and stability, which is unlike the chemically synthesized nanoparticles (Gurunathan et al. 2014). Gold nanoparticles occur in various size ranges from 2 to 100 nm, but 20–50 nm particles size range shows the most efficient cellular uptake. Specific cell toxicity is shown by 40–50 nm sized particles. These 40–50 nm particles diffuse into tumors and can be easily recovered. But the larger particles 80–100 nm do not diffuse into the tumor and stay near the blood vessels (El-Sayed et al. 2006). These have a great extinction coefficient (Alvarez et al. 1997). Thus, gold nanoparticles have a great contribution in cancer therapy, diagnosis of cancerous cell and importance in the therapy of HIV (Bowman et al. 2008). Colon cancer is the third most common cancer and the third leading cause of cancer death in men and women. In this study, we took colon cancer cell line and treated it with AuNPs–*C. tora* SMs conjugate to find its anticancer activity.

Materials and methods

Collection of plant material

Leaves of *C. tora* were collected from Cuddalore and Poonamallee, Chennai, Tamil Nadu, South India. It was authenticated by a plant taxonomist Preetam Raj JP from the Department of Plant Biology and Biotechnology, Loyola College, Chennai.

Bio-reduction of gold nanoparticles by *C. tora* leaves

Glasswares were rinsed with deionized water before starting the synthesis. $HAuCl_4$ was obtained from Sigma-Aldrich Chemicals. One gram of leaf powder was boiled in 10 ml of deionized water and subsequently filtered through Whatman No. 1 filter paper. An aliquot of 500 µl was taken and mixed with 99 ml of deionized water to that 1 ml of 1 mM $HAuCl_4$ was added. The mixture was kept on magnetic stirrer for 24 h.

Characterization of synthesized AuNPs

UV–Visible spectroscopy studies

UV–Vis spectroscopy measurements of the $HAuCl_4$ solution and *C. tora* SMs capped gold colloidal solution were carried out on a UV–Vis spectrophotometer (Model UV2450-Elico). Scanning was done from 200 to 800 nm.

Particle size analysis and zeta potential determination

The particle size ranges of the nanoparticles were determined using particle size analyzer (ZetasizerNano ZS-Malvern), and potential was measured using zeta potential. Particle sizes were calculated based on measuring the time-dependent fluctuation of scattering of laser light by the nanoparticles.

FT-IR spectroscopy measurements

After complete reduction of $HAuCl_4$ ions by *C. tora* SMs, the colloidal gold nanoparticles were centrifuged at 12,000 rpm for 10 min at room temperature. The gold nanoparticle pellet obtained after centrifugation was re-suspended in deionized water and centrifuged again to remove the traces of unbound leaf extract present in the solution prior to FT-IR analysis. FT-IR spectrum was taken to assess the involvement of possible capping by the plant extract (both aqueous and gold nanoparticles). Measurements were carried out on a Perkin–Elmer FT-IR Spectrum One spectrophotometer.

Dark field and HR-TEM measurements

Dark-field microscopy enables detailed studies of the plasmonic features of noble metal nanoparticles. AuNPs–*C. tora* SMs nominally sized 40–60 were used due to their stability. These particle qualities were diluted in essentially particle-free double-distilled H_2O and mixed to obtain suitable bimodal particle suspensions (Wagner et al. 2014). Olympus BX51 microscope was used which was illuminated with dark-field condenser. TEM samples of the gold nanoparticles were prepared by placing a drop over carbon-coated copper grid and allowing the solvent to evaporate. TEM measurements were performed on a TECHAN Philips model 2400EX instrument operated at an accelerating voltage between 80 and 200 kV.

Antibacterial activity

Test microorganisms

Bacillus subtilis (MTCC 441), *Enterococcus faecalis* (ATCC 29212), *Staphylococcus aureus* (ATCC 25923), *Staphylococcus epidermidis* (MTCC 3615), *Escherichia coli* (ATCC 25922) and *Proteus vulgaris* (MTCC 1771) were used for the experiment.

Well-diffusion assay

Antimicrobial activity was carried out using well-diffusion method. Petri plates were prepared with 20 ml of sterile Mueller-Hinton agar (MHA) (Hi-Media, Mumbai) for bacteria. The test cultures were swabbed on the top of the solidified media and allowed to dry for 10 min. The aqueous extract of *C. tora* leaves and synthesized *C. tora*–AuNPs (100 and 150 µl) were loaded and left for 30 min at room temperature for compound diffusion. $HAuCl_4$ $3H_2O$ was used as control. The plates were incubated for 24 h at 37 °C for bacteria to grow, and the zone of inhibition was measured in millimeters (mm). The experiment was repeated twice.

Anticancer activity

Col320 cell lines were obtained from National Centre for Cell Sciences, Pune, India, and grown on Dulbecco's modified essential medium supplemented with 10 % (v/v) fetal calf serum, penicillin (100 µ/ml) and streptomycin (100 µg/ml). Cells were seeded in 24 well plates at a concentration of 3×10^4 cells/ml of DMEM/well and incubated for 48 h at 37° C under 5 % CO_2 to attain confluence. The cells were then treated with various concentrations (25, 50 and 75 µg/ml). Then, the cells were incubated for 24 h, and cell supernatants (100 µl) were analyzed for leakage of catalase levels, using commercial spectrophotometric kits. The cells were used to analyze viability, NO production and lipid peroxidation. The experiments were carried out in triplicates in each group.

Estimation of cell viability—MTT assay

The MTT assay is a colorimetric assay for measuring the activity of cellular enzymes that reduce the tetrazolium dye, MTT, to its insoluble formazan, giving a purple color. MTT (3-4,5-dimethylthiazol-2-yl)-2,5-diphenyltetrazolium bromide, a yellow tetrazole) is reduced to purple formazan in living cells (Gerlier and Thomasset 1986; Mossman 1983). A solubilization solution (usually dimethyl sulfoxide, an acidified ethanol solution or a solution of the detergent sodium dodecyl sulfate in diluted hydrochloric acid) is added to dissolve the insoluble purple formazan product into a colored solution. The absorbance of this colored solution can be quantified by measuring at a certain wavelength (usually between 500 and 600 nm) by a spectrophotometer. Cell proliferation was measured using MTT assay. After 24 h of treatment, 20 µl of MTT solution (5 mg MTT in 1 ml PBS) was added per well and incubated at 37 °C for 4 h in 5 % CO_2 atmosphere. Then, the medium was removed and washed with PBS; 200 µl of DMSO was added to each well. The intensity of the colored product was measured using an ELISA microplate reader at 570/620 nm. The results were expressed as the percent optical density of treated cells to that of the control cell.

Estimation of catalase

To 0.1 ml of sample, 1 ml of phosphate buffer and 1 ml of hydrogen peroxide was added, and the timer was started. The reaction was arrested by the addition of 2 ml dichromate–acetic acid reagent. Standard hydrogen peroxide (20 µM) was taken and treated similarly. The tubes were heated in the boiling water bath for 10 min. The green color developed was read at 570 nm using spectrophotometer.

Assay for NO production

Nitric oxide (NO) plays an important role in neurotransmission, vascular regulation, immune response and apoptosis. NO is rapidly oxidized to nitrite and nitrate which are used to quantitate NO production. NO is a reactive radical that plays an important role in many key physiological functions. NO, an oxidation product of arginine by nitric oxide synthase (NOS), is involved in host defense and development, activation of regulatory proteins and direct covalent interaction with functional biomolecules. Simple, direct and non-radioactive procedures for measuring NOS are becoming popular in research and drug discovery. Nitric oxide synthase assay involves two steps: a NOS reaction step during which NO is produced followed by an NO detection step. Since the NO generated by NOS is rapidly oxidized to nitrite and nitrate, the NO production is measured following reduction of nitrate to nitrite using an improved Griess method. The procedure is reduced to as short as 40 min. This assay determines nitric oxide based on the enzymatic conversion of nitrate to nitrite by nitrate reductase. The reaction is followed by a colorimetric detection of nitrite as an azo dye product of the Griess reaction. The Griess reaction is based on the two-step diazotization reaction in which acidified NO_2 produces a

nitro-sating agent which reacts with sulfanilic acid to produce the diazonium ion. This ion is then coupled to N-(1-naphthyl) ethylenediamine to form the chromophoric azo derivative, which absorbs light at 540 nm. After 24 h of incubation, the level of NO production was monitored by measuring the nitrite concentration in the supernatant of cultured medium using the Griess reagent.

Estimation of lipoperoxides

Quantification of lipid peroxidation is essential to assess oxidative stress in pathophysiological processes. Lipid peroxidation forms malondialdehyde (MDA) and 4-hydroxynonenal (4-HNE), as natural by-products. Measuring the end products of lipid peroxidation is one of the most widely accepted assays for oxidative damage. Lipid peroxidation assay provides a convenient tool for sensitive detection of the MDA in a variety of samples. The MDA in the sample is reacted with thiobarbituric acid (TBA) to generate the MDA-TBA adduct. The MDA-TBA adduct can be easily quantified colorimetrically ($\lambda = 532$ nm) or fluorometrically (Ex/Em = 532/553 nm). This assay detects MDA levels as low as 1 nmol/well colorimetrically and 0.1 nmol/well fluorometrically. After treatment, the cells were trypsinized, suspended in 0.5 ml of PBS and sonicated for 10 s. To this, 0.5 ml of TCA–TBA reagent was added and heated to 100 °C for an hour and centrifuged. The extent of lipid peroxidation was quantified by estimating the levels of malondialdehyde. The absorbance was measured at 535 nm, and the results were expressed as nmol/mg protein (Wu and Cederbaum 2008).

Results and discussion

Characterization of synthesized AuNPs

Plasmon resonance

It is a useful technique to study the optical and electrical properties of the materials based on Beer–Lambert law which governs the absorption of light by molecules. Upon mixing the $HAuCl_4$ solution and *C. tora* leaf powder in deionized water, there was no significant change in the UV–Vis spectra (at 0 h), only the characteristic signature of *C. tora* leaf around 250 nm was seen, which we speculate may be due to complexation of Au^{3+} with *C. tora* leaf powder. Spectrophotometric absorption measurements in the wavelength ranges of 400–450 nm (Huang et al. 2007) and 500–550 nm (Shankar et al. 2004) are used in characterizing the silver and gold nanoparticles, respectively. As a function of time, we observed an emerging peak around 538 ± 2.82 nm (Fig. 1a), which was in the expected range. At this point of time, the color of the reaction mixture changed from gold to light purple color which is an indication of the formation of AuNPs. The formation of gold nanoparticles was visually confirmed by the color change (Fig. 1b). Such a color transition is often indicative of changes in the metal oxidation state (Fujiwara et al. 2007). The increase in the background may be due to the aggregation happened in the synthesized non-purified AuNPs–*C. tora* leaf conjugates (Choudhury et al. 2013). It is well known that the particles aggregate the background scattering. As one can observe the NPs formation after 2 h,

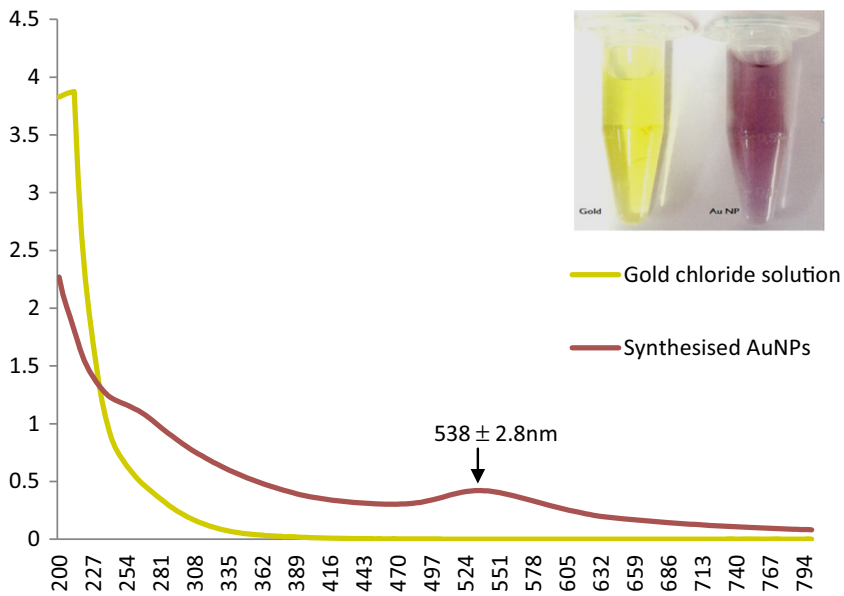

Fig. 1 UV–visible spectroscopy showing spectrum the of gold chloride solution at initial time and colloidal solution of AuNPs bioreduction of *C. tora* SMs after 24 h. *Inset* optical photograph of colloidal solution

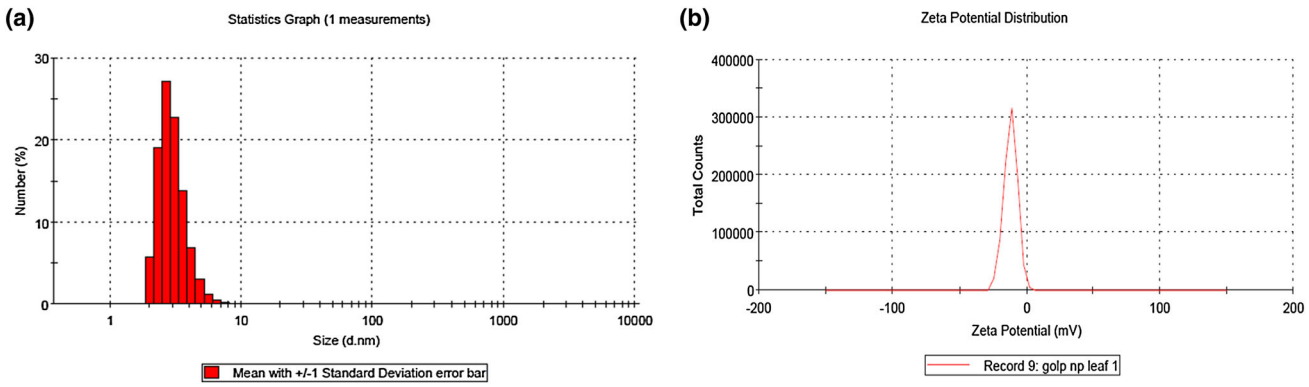

Fig. 2 **a** Particle size measurement **b** zeta potential measurement of AuNPs conjugated *C. tora* SMs

however, clear light purple color was observed by 24 h, indicating the completion of the reaction. More studies are required to prove the intermediates involved in the reaction. Following the UV–Vis spectroscopic study, we carried out FT-IR study to elucidate the possible structural modification in the *C. tora* leaf molecule, followed by TEM imaging, and zeta potential measurements were done to find the size and charge present on the slip plane of AuNPs.

Zeta sizer and potential

Zeta potential is the key parameter that controls electrostatic interactions in particle dispersions (Kaszuba et al. 2010). The zeta sizer and potential of AuNPs–*C. tora* conjugate were 41 nm and −12.5 mV (Fig. 2a, b). The negative potential is considered as an incipient stability for colloids (Ostolska and Wisniewska 2014). The AuNPs–*C. tora* conjugate colloidal solution was found to be stable for 3 month under refrigeration.

FT-IR

The qualitative aspects of infrared spectroscopy are one of the most powerful attributes of this diverse versatile analytical technique (Coates 2000). It is useful for characterizing the surface chemistry (Chithrani et al. 2006). We carried out FT-IR measurements in order to decipher the structural modifications occurred in *C. tora* leaf upon the formation of AuNPs conjugate. Conversely, one may be able to identify indirectly which moiety of *C. tora* leaf is bound to the AuNPs. IR spectroscopy, a vibrational spectroscopic technique, is known for elucidating the finger print of chemical compounds. We observed conspicuous peaks around 3464.15, 2926.01, 2395.59, 2011.76, 1622.13, 993.34, 844.82 and a peak around 561.29 cm^{-1}. The peaks around 3400 cm^{-1} are likely due to the alcohol OH stretch are usually a broad and strong absorption near 3400 and presence of residual water molecules in synthesized AuNPs. The peaks around 2750–3000 cm^{-1} are likely to originate from carbonyl C=O group which is present in the synthesized AuNPs. The peaks around 2300–2100 cm^{-1} indicate C≡X stretch region, the peaks around 1600–1750 cm^{-1} are likely due to the amide present in the synthesized AuNPs, and the peaks around 1500–400 cm^{-1} fingerprint region arise from complex deformations of the molecule. They may be characteristic of molecular symmetry, or combination bands arising from multiple bonds deforming simultaneously or the presence of peaklets at the lower wave numbers following it also could likely suggest the presence of aromatic C=C, which is present in synthesized AuNPs, also the disappearance of the peaklets at the lower wave number region after the formation of AuNPs suggests the possible structural change. Hence, peak around 1620 cm^{-1} is likely to be aliphatic (alkene) C=C also, whose absorption is converged with aromatic and amide absorption bands (Fig. 3a, b). Another potential structure is sharp, medium peak around 1400, and it signifies aromatic C=C group, but it shifted in synthesized AuNPs.

Dark field and HR-TEM

Dark-field microscopy is a widely unknown method to measure the particle size distribution of diffusing nanoparticles by particle tracking (Fig. 4a). TEM is used for morphological characterization at the manometer to micrometer scale. TEM measurements divulged that the resultant product after 24 h was comprised of nearly spherical AuNPs with 57 nm (Fig. 4b).

Antibacterial activity of synthesized AuNPs and aqueous *C. tora* leaf extract

The *C. tora* leaf may serve as a source of natural bactericidal agents to be used in medicinal systems (Koffi-Nevry

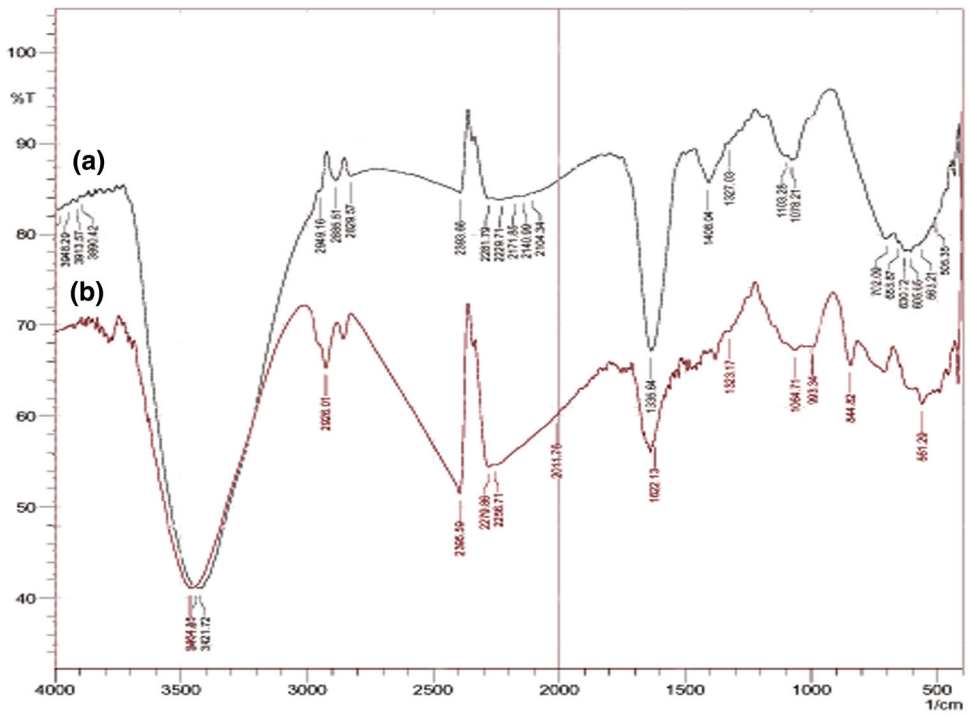

Fig. 3 Fourier transform infrared (FT-IR) absorption spectra (*a*) *C. tora* aqueous extract spectra, (*b*) AuNPs synthesized by bioreduction of *C. tora* SMs spectra

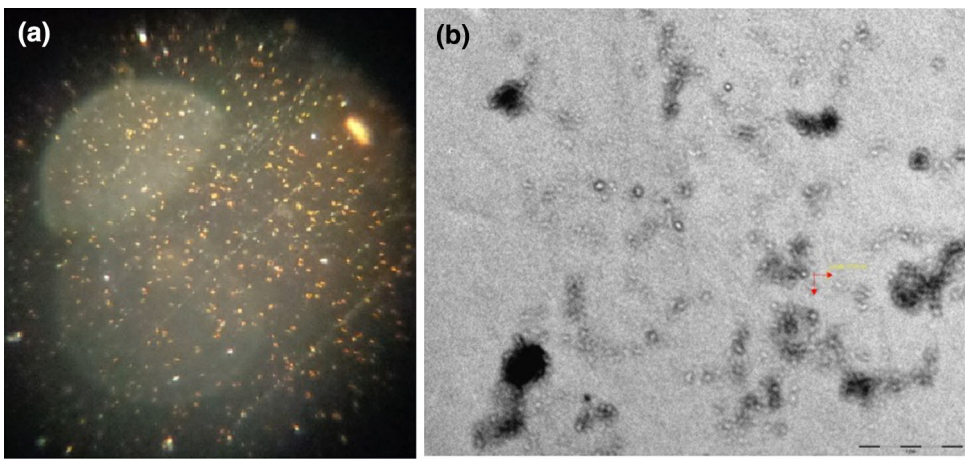

Fig. 4 **a** Gold colloidal particles under dark-field microscopy (×40), **b** HR-TEM image of synthesized AuNPs conjugated with *C. tora* SMs (*Scale bar* −1 μm)

et al. 2012). This study was designed to assess the antibacterial activity of synthesized AuNPs and aqueous *C. tora* leaf extract against gram-positive and gram-negative bacteria. The green synthesized AuNPs and aqueous *C. tora* leaf extract showed no inhibition against the gram-positive bacteria and gram-negative bacteria.

Anticancer activity

We intended to use AuNPs capped with *C. tora* leaf extract on cancer cells to observe the enhanced bioavailability and anticancer activity of *C. tora* focusing on colon cancer cell line. Col320 is widely used due to its relatively high steady state functioning of the free radical production and antioxidant defenses; therefore, variations of responses at different conditions are more easily detected.

Estimation of cell viability

The anticancer activity of the extract was confirmed by MTT assay. The measurement of cell viability plays a fundamental role in all forms of cell culture (Stoddart 2011). Promoting appropriate cell life and death is a key part of cell culture. When cells are put into contact with a SM, their viability may be affected. Some materials are cytotoxic, i.e., deadly to cells. In the present study, the treatment of Col320 cell line with the AuNPs capped with *C. tora* leaf extract suppressed the cell viability of

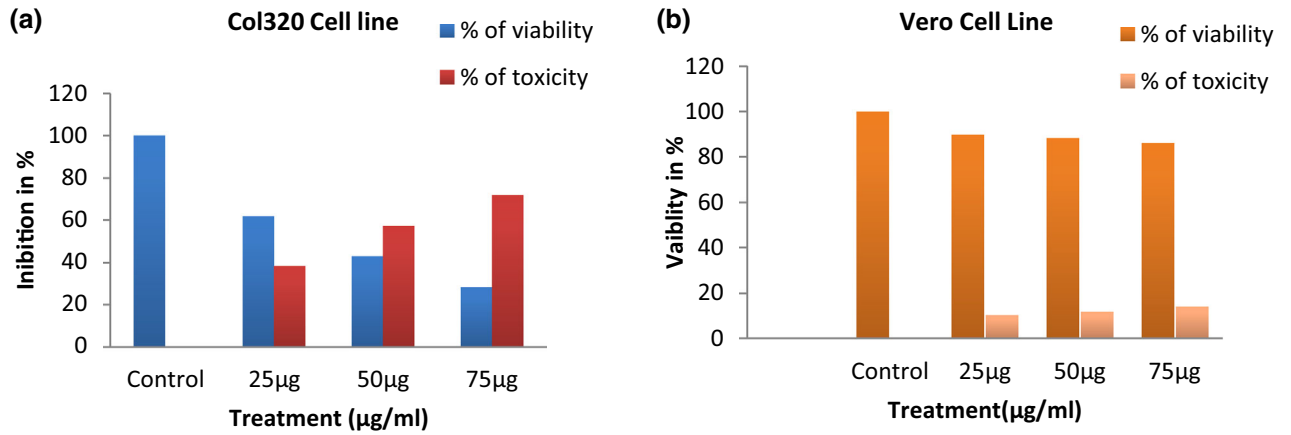

Fig. 5 Graph showing the effect of AuNPs conjugate *C. tora* on **a** colon cancer (Col320) and **b** cell line and Vero cell lines

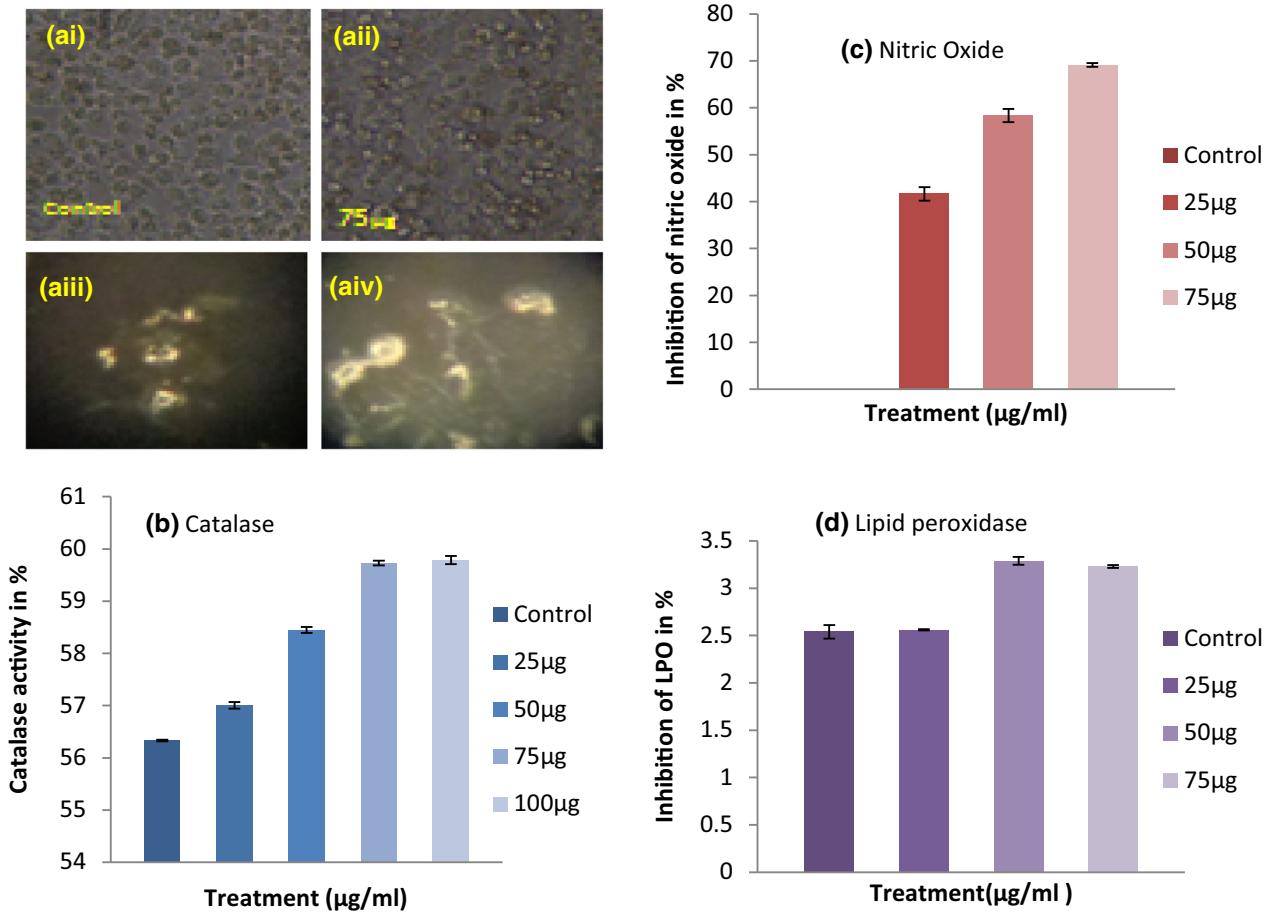

Fig. 6 **a** Col320 cell lines after 24 h of incubation **ai** control, **aii** AuNPs–*C. tora* conjugate 75 µg, **aiii** dark-field image showing nanoparticles in the Col320 apoptosis cells ×10 and **aiv** dark-field image at ×40, **b** catalase activity, **c** nitric oxide inhibition and **d** lipid peroxidase activity

cancerous cell up to (71.2 %) at (75 µg) concentrations when compared to the untreated cells (Fig. 5a). Cell morphological changes such as cell shrinkage, loss of surface contact and blebbing were observed in treated cancer cells Col320 cell lines after 24 h of incubation [Fig. 6a(i, ii)]. Cells were also observed in dark-field microscope [Fig. 6a(iii, iv)]. And we also checked the toxicity of the AuNPs capped *C. tora* leaf extract on normal cell line (Vero), and it is found that our sample does not affect the viability of normal cell (Fig. 5b). Hence, our results

confirm that the *C. tora* leaf extract conjugated with AuNPs shows higher activity and can be used to enhance activity of colon cancer.

Catalase assay

To confirm the anticancer activity further, catalase was carried out; catalase is a ubiquitous antioxidant enzyme that degrades hydrogen peroxide into water and oxygen (Loewen et al. 1985), and H_2O_2 is very dangerous to the cells and tissues. In our study, when the concentration of the AuNPs capped *C. tora* leaf extract increased, it showed gradual increase in catalase enzyme, and when enzyme increases, it breaks H_2O_2 present in the cancerous cells, and hence, H_2O_2 is reduced into non-toxic molecules like water and oxygen (Fig. 6b).

Assay for NO production

Production of NO molecules is an important cytotoxic function that macrophages use to resolve infection by several obligate intracellular protozoan and bacterial parasites (De Groote and Fang 1995). The inducible form of the NO synthase enzyme (iNOS) produces large amounts of reactive nitrogen molecules by oxidizing the terminal guanidino nitrogen of L-arginine (Dong et al. 1995; Park et al. 1996). Since reactive nitrogen molecules can damage host tissues as well as the invading microbe (Park et al. 1996), nitric oxide at appropriate levels is involved in normal function of organs, whereas uncontrolled release can cause destruction of target tissue during inflammation and septic shock (Saravanan et al. 2012). The treatment with AuNPs–*C. tora* leaf conjugates (75 µg) significantly reduced the release of NO (69.12 µM) (Fig. 6c). Low level of NO is important in protecting organs; hence, our sample is capable for reducing NO in the cells and helps in protecting the cells.

Estimation of lipoperoxide

The major reactive aldehyde resulting from the peroxidation of biological membranes is malondialdehyde (MDA; Vaca et al. 1988). It is used as an indicator of tissue damage by a series of chain reactions (Ohkawa et al. 1979). Malondialdehyde, being a major breakdown product of lipid peroxides, is a useful index of lipid peroxidation (Saravanan et al. 2013). The treatment with AuNPs–*C. tora* leaf conjugates reduced the release of LPO (3.23). Thus, the study confirmed the anticancer property of AuNPs–*C. tora* through modulating the free radicals release and also established anti-inflammatory potential (Fig. 6d).

Conclusion

Aqueous extract of *C. tora* lacks in bioavailability and permeability, mainly due to its poor solubility of extract in water. To improve the bioavailability of *C. tora*, it is conjugated to the surface of metal nanoparticles. In the present study, we report the binding of *C. tora* to the surface of AuNPs. The nanoparticles were characterized by zeta sizer, TEM and FT-IR. We found that *C. tora* acts both as a reducing and capping agent, stabilizing the gold solution. The synthesized AuNPs–*C. tora* SMs conjugate showed enhanced bioavailability, antioxidant and anticancer effect against colon cancer cell line (Col320). To the best of our knowledge, this is the first report to describe the synthesis of biocompatible and soluble AuNPs with an average size of 41 nm using *C. tora*. Therefore, this study could provide valuable insight in using AuNPs capped *C. tora* leaf extract as a potential anticancer agent. Further, various parts of this medicinal plant could be explored using nanotechnology for assessing its therapeutic potential.

References

Alvarez MM, Khoury JT, Schaaff TG, Shafigullin MN, Vezmar I, Whetten RL (1997) Optical absorption spectra of Nanocrystal gold molecules. Phys Chem B 101:3706–3712. doi:10.1021/jp962922n

Bowman M, Ballard TE, Ackerson CJ, Feldheim DL, Margolis DM, Melander C (2008) Inhibition of HIV fusion with multivalent gold nanoparticles. J Am Chem Soc 130:6896–6897. doi:10.1021/ja710321g

Cai W, Chen X (2007) Nanoplatforms for targeted molecular imaging in living subjects. Small 3:1840–1854. doi:10.1002/smll.200700351

Chen S, Li G, Zhu K, Sun P, Wang R, Zhao X (2014) Antitumor activities of Juemingzi (*Cassia tora* L.) on Balb/c sarcoma 180-injected mice. Oncol Lett 7(1):250–254

Chithrani BD, Ghazani AA, Chan WCW (2006) Determining the size and shape dependence of gold nanoparticle uptake into mammalian cells. Nano Lett 6:662. doi:10.1021/nl052396o

Choudhury D, Xavier PL, Chaudhari K, John R, Dasgupta AK, Pradeep T, Chakrabarti G (2013) Unprecedented inhibition of tubulin polymerization directed by gold nanoparticles inducing cell cycle arrest and apoptosis. Nanoscale 5:4476–4489. doi:10.1039/C3NR33891F

Coates J (2000) Interpretation of infrared spectra: a practical approach. In: Meyers RA (ed) Encyclopedia of analytical chemistry. Wiley, Chichester, pp 10815–10837

Cordova CA, Siqueira IR, Netto CA, Yunes RA, Volpato AM, CechinelFilho V, Curi-Pedrosa R, Creszynski-Pasa TB (2002) Protective properties of butanolic extract of the *Calendula officinalis* L. (marigold) against lipid peroxidation of rat liver

microsomes and action as free radical scavenger. Redox Rep 7:95–102. doi:10.1179/135100002125000325

De Groote MA, Fang FC (1995) NO inhibitions: antimicrobial properties of nitric oxide. Clin Infect Dis 21(Suppl 2):S162–S165. doi:10.1093/clinids/21.Supplement_2.S162

Dong Z, Yang X, Xie K, Juang S-H, Llansa N, Fidler IJ (1995) Activation of inducible nitric oxide synthase gene in murine macrophages requires protein phosphatases 1 and 2A activities. J Leukoc Biol 58:725–32. http://www.jleukbio.org/content/58/6/725.full.pdf+html

El-Sayed I, Huangand X, El-Say AM (2006) Selective laser photothermal therapy of epithelial carcinoma using anti-EGFR antibody conjugated gold nanoparticles. Cancer Lett 2:129–135. doi:10.1016/j.canlet.2005.07.035

Fujiwara K, Ramesh A, Makia T, Hasegawaa H, Ueda K (2007) Adsorption of platinum (IV), palladium (II) and gold (III) from aqueous solutions onto L-lysine modified cross linked chitosan resin. J Hazard Mater 146:39–50. doi:10.1016/j.jhazmat.2006.11.049

Gerlier D, Thomasset N (1986) Use of MTT colorimetric assay to measure cell activation. J Immunol Methods 94:57–63. doi:10.1016/0022-1759(86)90215-2

Gurunathan S, Han J, Park JH, Kim JH (2014) A green chemistry approach for synthesizing biocompatible gold nanoparticles. Nanoscale Res Lett 9:248. doi:10.1186/1556-276X-9-248

Harrison D (2003) Natural therapeutic composition for the treatment of wounds and sores. CIPO Patent 2392544

Horvath F (1992) Therapeutical compositions against psoriasis. US Patent 5165932

Huang J, Li Q, Sun D, Lu Y, Su Y, Yang X, Wang H, Wang Y, Shao W, He N, Hong J, Chen C (2007) Biosynthesis of silver and gold nanoparticles by novel sundried *Cinnamomum camphora* leaf. Nanotechnology 18(10):105104–105115. doi:10.1088/0957-4484/18/10/105104

Kaszuba M, Corbett J, Watson FM, Jones A (2010) High-concentration zeta potential measurements using light-scattering techniques. Philos Trans A Math Phys Eng Sci 368(1927):4439–4451. doi:10.1098/rsta.2010.0175

Koffi-Nevry R, Kouassi KC, Nanga ZY, Koussémon M, Loukou GY (2012) Antibacterial activity of two bell pepper extracts: *Capsicum annuum* L. and *Capsicum frutescens*. Int J Food Prop 15(5):961–971. doi:10.1080/10942912.2010.509896

Loewen PC, Switala J, Triggs-Raine BL (1985) Catalases HPI and HPII in *Escherichia coli* are induced independently. Arch Biochem Biophys 243:144–149. doi:10.1016/0003-9861(85)90782-9

Mossman T (1983) Rapid colorimetric assay for cellular growth and survival: application to proliferation and cytotoxicity assays. J Immunol Methods 65:55–63. doi:10.1016/0022-1759(83)90303-4

Ohkawa H, Ohishi N, Yagi K (1979) Assay for lipid peroxidation in animal tissues by thiobarbituric acid reaction. Ann Biochem 95:351–358

Ostolska I, Wiśniewska M (2014) Application of the zeta potential measurements to explanation of colloidal Cr_2O_3 stability mechanism in the presence of the ionic polyamino acids. Colloid Polym Sci 292(10):2453–2464. doi:10.1007/s00396-014-3276-y

Park YC, Jun CD, Kang HS, Kim HD, Kim HM, Chung HT (1996) Role of intracellular calcium as a priming signal for the induction of nitric oxide synthesis in murine peritoneal macrophages. Immunology 87:296–302. doi:10.1046/j.1365-2567.1996.456544.x

Qi GF (2011) Cassia analysis of lipid-lowering active ingredients. Guang Ming Zhong Yi 26:1569–1570

Saravanan S, Babu NP, Pandikumar P, Raj MK, Paulraj MG, Ignacimuthu S (2012) Immunomodulatory potential of Enicostema axillare (Lam.) A. Raynal, a traditional medicinal plant. J Ethnopharmacol 140:239–246. doi:10.1016/j.jep.2012.01.010

Saravanan S, Pandikumar P, Pazhanivel N, Gabriel Paulraj M, Ignacimuthu S (2013) Hepatoprotective role of *Abelmoschus esculentus* (Linn.) Moench on carbon tetrachloride induced liver injury. Toxicol Mech Methods 23(7):528–536. doi:10.3109/15376516.2013.796032

Sathya A, Ambikapathy V (2012) Studies on the phytochemistry, antibacterial activity and green synthesis of nanoparticles using *Cassia tora* L. against amphicillin resistant bacteria. Asian J Plant Sci Res 2(4):486–489. http://pelagiaresearchlibrary.com/asian-journal-of-plant-science/vol2-iss4/AJPSR-2012-2-4-486-489.pdf

Shankar SS, Rai A, Ankamwar B, Singh A, Ahmad A, Sastry M (2004) Biological synthesis of triangular gold nanoprisms. Nat Mater 3:482–488. doi:10.1038/nmat1152

Stary F, Hans S (1998) The National guides to medical herbs and plants. Tiger Books Int. Plc, UK

Stoddart MJ (2011) Cell viability assays: introduction. Methods Mol Biol 740:1–6. doi:10.1007/978-1-61779-108-6_1

Vaca CE, Wilhelm J, Harms-Ringdahl M (1988) Interaction of lipid peroxidation products with DNA: a review. Mutat Res 195:137–149. doi:10.1016/0165-1110(88)90022-X

Wagner T, Lipinski HG, Wiemann M (2014) Dark field nanoparticle tracking analysis for size characterization of plasmonic and non-plasmonic particles. J Nanopart Res. doi:10.1007/s11051-014-2419-x

Wu D, Cederbaum A (2008) Cytochrome P4502E1 sensitizes to tumor necrosis factor alpha-induced liver injury through activation of mitogen-activated protein kinases in mice. Hepatology 47(3):1005–1017. doi:10.1002/hep.22087